Available online at www.sciencedirect.com

SciVerse ScienceDirect

Ceramics International 38 (2012) 6243–6252

CERAMICS INTERNATIONAL

www.elsevier.com/locate/ceramint

Effect of processing route on the properties of Ni-based catalytic filters obtained from natural amorphous silica fibers

K. Donadel[a], C.R. Rambo[a,*], W.S. Chacon[c], M.D.M. Innocentini[c], R.C. Catapan[b], D. Muller[a], A.A.M. Oliveira[b], A.P.N. Oliveira[a]

[a]*Group of Ceramic and Glass Materials, Florianópolis, Brazil*

[b]*Laboratory of Combustion and Thermal Systems Engineering, Federal University of Santa Catarina (UFSC), P.O. Box 476, 88040-900 Florianópolis (SC), Brazil*

[c]*Undergraduate Program on Chemical Engineering, University of Ribeirão Preto (UNAERP), Av. Costábile Romano, 2201, Ribeirânia, 14096-900 Ribeirão Preto (SP), Brazil*

Received 16 January 2012; received in revised form 26 April 2012; accepted 27 April 2012
Available online 8 May 2012

Abstract

In this work catalytic fibrous filters were produced through two distinct processing routes from natural amorphous silica fibers (NASF) and $Ni(NO_3)_2$ solution (wet route) and NiO (dry route) as catalyst precursors. The Ni–SiO_2 fibers were characterized for X-ray powder diffraction, scanning electron microscope, particle size distribution, specific surface area, nickel contents, porosity, tortuosity, permeability, compressive strength, degree of dispersion, filtration and gas conversion efficiency. Morphological characterization revealed that Ni from wet route was distributed over the silica fibers with significantly lower particle size than the Ni produced through the dry route. Both methods led to a homogeneous distribution of Ni. The catalytic fibrous filter obtained from the dry route showed higher conversion efficiency for both propylene and propane, especially at high temperatures, due to the higher degree of dispersion of Ni particles over the NASF surfaces.
© 2012 Elsevier Ltd and Techna Group S.r.l. All rights reserved.

Keywords: Catalytic filters; Natural amorphous silica fibers; Conversion efficiency; Permeability

1. Introduction

The environmental problems generated by atmospheric pollution demand new green technologies that require highly efficient separation and cleaning techniques for pollutants released from combustion processes such as particulates as well as unburned hydrocarbons, CO and NO_x. The continuous tightening of emissions regulations for the mobility sector has been possible due to the continuous advances in in-cylinder control of formation of pollutants and the development of effective underfloor filters and catalytic converters. Different alternatives for particulate filters and catalysts have been developed in the last two decades in order to achieve the emission limits established by national and international legislation [1–5].

Catalytic filters combine filtration and catalytic reactions in a single unit in a way that the processing costs, investments and maintenance are reduced. The particulates in the gases are initially captured on the filter surface and the undesirable gases are treated during flow through the catalytic surface [6,7]. The use of ceramic substrates is necessary since the gas temperature during normal operation of diesel engines ranges from ambient, in cold-start, up to 1000 K during the regeneration cycle of wall flow particulate traps. Normal temperatures for catalysis of pollutants emitted from internal combustion engines range from 500 K to 700 K [8].

The catalytic activity and selectivity of a supported catalyst is influenced by several factors such as catalyst preparation, support composition, metal loading, size and shape of dispersed metal particles, active phase, and precursor employed as well as pretreatment. Different routes can be applied to obtain highly dispersed metals

*Corresponding author.
E-mail address: rambo@enq.ufsc.br (C.R. Rambo).

0272-8842/$36.00 © 2012 Elsevier Ltd and Techna Group S.r.l. All rights reserved.
http://dx.doi.org/10.1016/j.ceramint.2012.04.078

on support surface. The precursor compounds used for the catalyst preparation have a key role in catalytic performance [9,10]. Supported nickel catalysts have been widely used industrially in reforming of natural gas [11,12] and methanation [13,14], mainly due to their commercial low cost and high activity for C–H bond breaking of the methane [12]. Supported nickel catalyst can be prepared using high metal loading, typically around 20 wt%, however, getting a highly dispersion catalyst is a challenge due to the trend of nickel for sintering in high temperatures [11]. The most usual routes for the preparation supported nickel catalysts are impregnation with salts, ion-exchange and precipitation–deposition of nickel precursors on the supports [10,15].

The filtration efficiency is an important characteristic of filters used to remove aerosol particles. Fibrous media filters are widely used with high efficiency in the cleaning of suspended particles [16]. However, the fibrous structures of filters for removal of aerosol particles are complex and difficult to model. The filtration efficiency is function of several variables, such as, structure of the filtering media (porosity, pore size distribution, fibers diameter and medium thickness), of the aerosol properties (mass concentration, dust size distribution, particle and gas density and gas viscosity) and of the operation parameters (temperature, humidity and filtration velocity). Variations in the parameters of the filters in order to increase filtration efficiency are usually accompanied by an increase of pressure drop [16–18]. Therefore, *in-situ* measurements of these properties are required to develop catalytic filters.

In this context, this work reports the processing and characterization of Ni-based catalytic fibrous filters by two distinct routes. The effect of the processing routes on the filter physical properties and catalysis efficiency was evaluated.

2. Materials and methods

The Ni-based catalytic filters were prepared by two distinct routes, here named wet and dry routes, using natural amorphous silica fibers (NASF) as support. Natural amorphous silica fibers (NASF) are obtained from spongillite ore, and exhibit a cylindrical shape. The spongillite is composed particularly of siliceous spicules (small needles composed of amorphous hydrated silica or opal), associated with clay, grains of sand, shells of diatoms and organic matter. These spicules are inorganic constituents of the support structure of the body of fresh water sponges [19,20]. The NASF used in this work were provided by São Caetano Ceramic Ltda (Brazil-SC).

In the dry route, NASF, 5 wt% bentonite (Colorminas-Brazil-SC) and 5 wt% of NiO (Vetec) were dry mixed, humidified (10%) and uniaxially pressed at 5.4 MPa. The green compacts were then heated up to 500 °C for 60 min at 5 °C/min in a 5%H_2/95%N_2 atmosphere for reduction of NiO, followed by a temperature increasing up to 1000 °C at 10 °C/min for 60 min in N_2 atmosphere. For the wet route aqueous suspensions containing NASF and 5 wt% bentonite were prepared, homogenized, dried and disaggregated. The powder was added to a 0.5 M nickel nitrate solution $Ni(NO_3)_2$ (Vetec), stirred and heated at 100 °C for 3 h. The dry powder from the wet route was then uniaxially pressed at 5.4 MPa and the compacts were sintered at 1000 °C for 60 min in N_2 atmosphere.

The true (or solid) density (ρ_t) of the sintered samples was measured by using a He-picnometer and the apparent density (ρ_{ap}) was obtained by mass and size measurements. Porosity (ε) was calculated according to Eq. (7).

$$\varepsilon = [1-(\rho_{ap}/\rho_t)] \cdot 100 \quad (1)$$

The specific surface area (S_{BET}) was measured by BET (Quantachrome analyzer-Model Nova 1200) using N_2 adsorption at 77 K. Scanning electron microscope (SEM) (Philips—Model XL-30) was used for morphological and microstructure analysis. Particle size distribution was obtained by image analysis—IMAGO®. To investigate the crystalline phases formed during heat treatments, samples were analyzed with a powder diffractometer (XRD Philips X'Pert) with radiation Cu-Kα ($\lambda = 1.54$ Å), generated in 40 KV and 30 mA. The nickel loading in each catalyst was measured by inductively coupled plasma mass spectroscopy (ICP-MS) (Perkin Elmer SCIEX, ELAN 6000). Compressive strength was measured in a universal test machine (EMIC-Model DL 2000) with a test speed of 1 mm/min. The degree of dispersion was estimated through image analysis (SizeMeter, Software Solutions, v.1.1) of three binarized SEM micrographs of each route by measuring the average distance between a selected particle and its first neighbors. A set of 10 randomic particles for each measurement was used for statistical counting. The coefficient of variation (C_υ) was used as parameter that indicates the degree of dispersion. It is defined as the ratio of the standard deviation σ to the mean ζ ($C_\upsilon = \sigma/\zeta$). In this case the evaluation of dispersion is made in terms of the mean distance between particles. For a homogeneous distribution, *i.e.*, well dispersed particles, σ approaches to zero. X-ray photoelectronic spectroscopy (XPS) (ESCA3000, V.G. Microtech) was applied to analyze the Ni deposited on the surface of NASFs. The measurements were performed using MgKα radiation (1253.6 eV) in an ultrahigh vacuum chamber at 10^{-9} mbar. The data were evaluated with the XPSPEAK41 software.

Permeability parameters were obtained experimentally and based on Forchheimer's Eq. (8), an empirical relationship that expresses the parabolic dependence of pressure drop (ΔP) through the medium with the superficial velocity (v_s) [21–23].

$$\frac{\Delta P}{L} = \frac{\mu}{k_1} v_s + \frac{\rho}{k_2} v_s^2 \quad (2)$$

For compressible flow, assuming ideal gas behavior, ΔP is obtained from Eq. (9).

$$\Delta P = \frac{P_i^2 - P_o{}^2}{2P} \quad (3)$$

where P_i and P_o are, respectively, the absolute fluid pressures at the entrance and exit of the medium, L is the medium length or thickness along the macroscopic flow direction, μ and ρ are, respectively the gas dynamic viscosity and density. The superficial or face velocity v_s is the volumetric flow rate Q divided by the nominal face area of the sample exposed to flow, A_{flow}. P is the absolute pressure (either P_i or P_o) for which v_s, μ and ρ are calculated. The terms k_1 and k_2 are referred as Darcian and non-Darcian permeability coefficients or constants [21,24]. k_1 is related to microscopic resistance to viscous flow in absence of inertia effects while k_2 reflects the growing importance of microscopic inertia effects as the pore Reynolds number increase.

The experimental evaluation of permeability was carried out at room conditions and also at temperatures up to 450 °C, in tests in which air was forced to flow through the porous samples in stationary regime. The sample was laterally sealed between two chambers and flow was controlled by a valve. Pressure drop ($P_i - P_o$) was measured by a digital micromanometer (Gulpress 200, Instrutemp) and recorded as a function of the air volumetric flow rate Q, measured with rotameters (0–40 L/min) and soap-bubble flow meters (0–10 L/min) and converted to the superficial velocity by $v_s = Q/A_{\text{flow}}$. The whole system (chambers and sample-holder) was set within an electric furnace (7500 W) controlled by a PID system, which allows programming up to 10 heating rates and 10 temperature plateaus. The air flow was pre-heated in a 2 m-long metal-coil within the furnace chamber before reaching the sample. Temperature was measured with K-type thermocouples situated normal to the sample at entrance and exit chambers. Thermocouples were also used to monitor the air temperature near the pressure transducers and prior to entering in the flowmeter devices. The exit measured temperature was used for calculations of air density and viscosity.

For the tests, firstly the sample was tightly fixed in the sample-holder using heat-resistant O-rings to avoid leakage. The temperature was raised to the desired point and air allowed to flow upwards through the sample with a constant pressure P_i. When the steady-state regime was reached (constant T, P_i and P_o), the volumetric flow rate Q was measured at the sample exit. Three flow rate measurements were carried out for each pressure setting at a given temperature. After the collection of at least 10 pairs of pressure and flow rate data, the temperature was raised and the whole procedure repeated. The collected data set ($\Delta P \times v_s$) was treated according to the least-square method using a parabolic model of the type: $y = ax + bx^2$, in which y is ΔP (from Eq. (9)) and x is the fluid velocity v_s. The permeability parameters of Forchheimer's equation (Eq. (8)) were then calculated from the fitted constants a and b, respectively by $k_1 = \mu/a$ and $k_2 = \rho/b$.

Changes in fluid properties were considered for the evaluation of permeability coefficients. Both air density (ρ_{air}) and air viscosity (μ_{air}) were corrected with temperature (T) assuming ideal gas behavior and using Eqs. (4) and (5) [21].

$$\rho_{air}(T) = \rho_r \frac{T_r}{T}\frac{P}{P_r} \tag{4}$$

$$\mu_{air}(T) = 1.73 \times 10^{-5}\left(\frac{T}{273}\right)^{1.5}\left(\frac{398}{T+125}\right) \tag{5}$$

where ρ_r is the air density at the temperature T_r and pressure P_r of reference (in this work, $\rho_r = 1.29$ kg/m^3 at $T_r = 273$ K and $P_r = 1.013 \times 10^5$ Pa). T is the average air temperature between entrance and exit of the sample.

An equivalent transport pore diameter was also obtained for the tested samples from permeability and tortuosity data. Such approach is very common to predict equivalent pore sizes in soils and basically involves the application of a parallel capillary model to the permeation in the porous medium [25]. The equivalent transport pore diameter (d_{transp}) is defined as the diameter of a straight tube in which a Poiseuille flow would result in the same ratio between Darcy permeability, porosity and tortuosity as the flow in the porous medium [25–27], *i.e.*,

$$d_{transp} = \left(\frac{32k_1}{\varepsilon/\tau}\right)^{0.5} \tag{6}$$

where ε is the porosity and τ is the tortuosity.

Eq. (6) neglects variations in pore diameter, pore length, connectivity and surface effects and for this reason is expected to be an average value for the whole structure. The range of validity for this equation is within the Darcy flow regime, where the influence of k_1 predominates [26].

2.1. Filtration efficiency

The filtration tests were performed at room temperature using a ground phosphate concentrate with nominal density of 2.75 g/cm^3 and average diameter of 20 μm as the particles to be captured. An aerosol stream was generated in a fluidized bed generator and introduced by suction provided by a vacuum pump downstream from the filter. Filtration velocity was kept at 1.1 cm/s with help of a control valve, within the range recommended for hot gas filtration in industrial applications (1 to 5 cm/s). Only the overall filter efficiency was evaluated. Filtration time was fixed at 10 min and only one cycle was performed for each sample. The aerosol flow exiting the filter was bubbled into a water column with surfactant to retain the passing dust particles. Measurements of turbidity were performed before and after filtration. A calibration curve previously prepared with different dust loads was used to obtain the actual aerosol mass concentration at the filter exit.

2.2. Catalytic efficiency

The experimental setup used to evaluate the catalytic efficiency is described schematically in Fig. 1. It is composed by an atmospheric pressure, stainless steel reactor with 30 mm of diameter, a furnace, flow rate controllers, gas mixtures

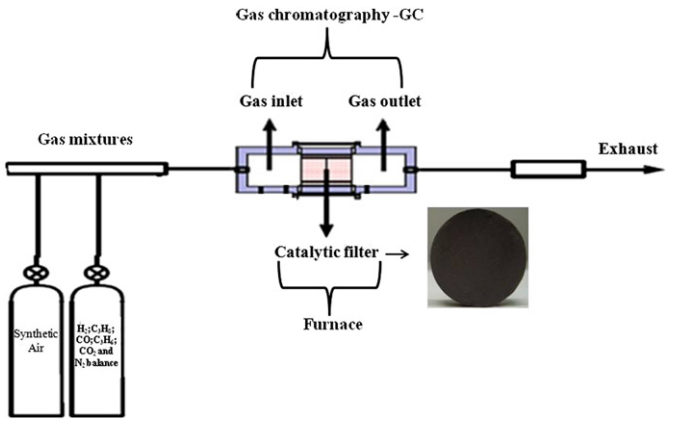

Fig. 1. Schematic drawing of the experimental setup used to evaluate the catalytic efficiency.

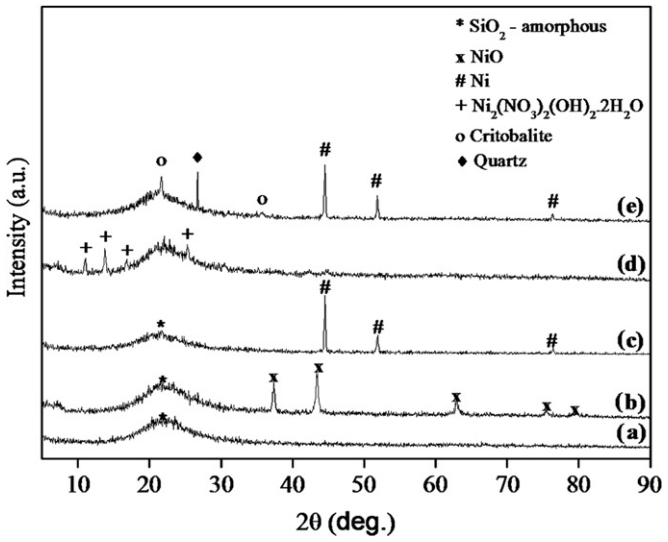

Fig. 2. X-ray diffraction patterns of: (a) NASF; (b) green Ni–SiO_2 fibers (dry route); (c) reduced Ni–SiO_2 fibers (dry route); (d) green Ni–SiO_2 fibers (wet route); (e) reduced Ni–SiO_2 fiber (wet route).

containing C_3H_8, C_3H_6, CO, CO_2, H_2, N_2 and synthetic air. A sample with approximately 7.0 g of the catalytic fibrous filters was used in each test. The experimental procedure is explained below. First, the temperature of the reactor was increased until 150 °C under a flow of N_2 (40 mL/min) and kept at this temperature for 60 min under a flow of 5%H_2/95%Ar (40 mL/min). The temperature was increased until the desired reaction temperature under a flow of N_2. Then, the system was fed with equal parts of a gas mixture composed: 503 ppm of C_3H_8, 0.3% of C_3H_6, 954 ppm of CO, 25% of CO_2, 311 ppm of H_2, balanced in N_2, and synthetic air (20% O_2), with a total gas flow rate of 1.33 L/min. Sampling of the gas-phase reactants and products were made with the aid of a gastight syringe at the same conditions and at temperatures of 150 °C, 300 °C and 500 °C.

The quantitative analysis of the main gas-phase species were carried out in gas chromatograph (Agilent, model 6890) equipped with thermal conductivity detector (TCD). The gases were analyzed with two different columns, Porapak *Q* (for C_3H_8 and C_3H_6) and Molesieve (for CO). Helium was used as carrier gas in both columns with a constant velocity of 40 cm/s.

3. Results and discussion

The XRD patterns for NAS fibers, green and reduced Ni-based catalyst supported on natural amorphous silica fibers for dry and wet routes are shown in Fig. 2. The broad halo at around 22° in the pattern (a) is related to amorphous SiO_2. The diffractograms (b) and (c) refer to Ni–SiO_2 fibers obtained by dry route before and after reduction, respectively. Before reduction only amorphous silica and NiO (ICDD PDF card 04-835) were detected. After reduction metallic nickel (ICDD PDF card 04-850) was formed. The diffractograms (d) and (e) refer to Ni–SiO_2 fibers obtained through the wet route before and after reduction, respectively. Before reduction nickel nitrate hydroxide hydrate ($Ni_2(NO_3)_2(OH)_2 \cdot 2H_2O$) (ICDD PDF card 27-0952) was detected together with amorphous silica. After reduction, however, metallic nickel (ICDD PDF card 04-850) was formed, but quartz (ICDD PDF card 85-0797) and cristobalite (ICDD PDF card 27-0605) were also detected. The crystallization of quartz and cristobalite in the wet route are probably related to a water vapor atmosphere formed during heat treatment. When ceramic systems containing liquid silicates are submitted to high water vapor containing atmospheres a decrease in the vitrification temperature occurs, which causes the decrease of the liquid silicate viscosity and as a consequence a decrease in the crystallization temperature of the phases present in the system [28]. The absence of peaks attributed to silicates in all spectra indicates that there is no apparent interaction between the nickel catalysts and NASF.

Fig. 3 shows SEM micrographs of NAS fibers, commercial nickel oxide and the deposited precursors on SiO_2 fibers for by dry and wet routes before annealing, respectively. According to the SEM observations, the NAS fibers (Fig. 3a) are characterized by an acicular shape with a mean diameter of 10 μm and lengths ranging from 200 to 600 μm. Moreover, the silica fibers are hollow with inner diameters below 1 μm. Fig. 3b shows micrographs of a commercial nickel oxide powder. Agglomerates composed of spherical particles with average particle size of 65 nm can be observed. Fig. 3c and d show micrographs of the precursors deposited onto the SiO_2 fibers by wet and dry routes, respectively. The particles of both precursors are coating the NAS fibers. NiO particles exhibit sizes below 1 μm, while nitrate deposited particles are present in an acicular morphology with sizes in the order of 1 μm.

Fig. 4 shows SEM micrographs of the Ni coated NASFs after annealing. No significant morphoilogical changes could be observed on the fibers after heat treatment. A higher magnification of the fibers surface revealed that particles of Ni produced through the dry route were homogeneously distributed over the NAS fibers (Fig. 4b).

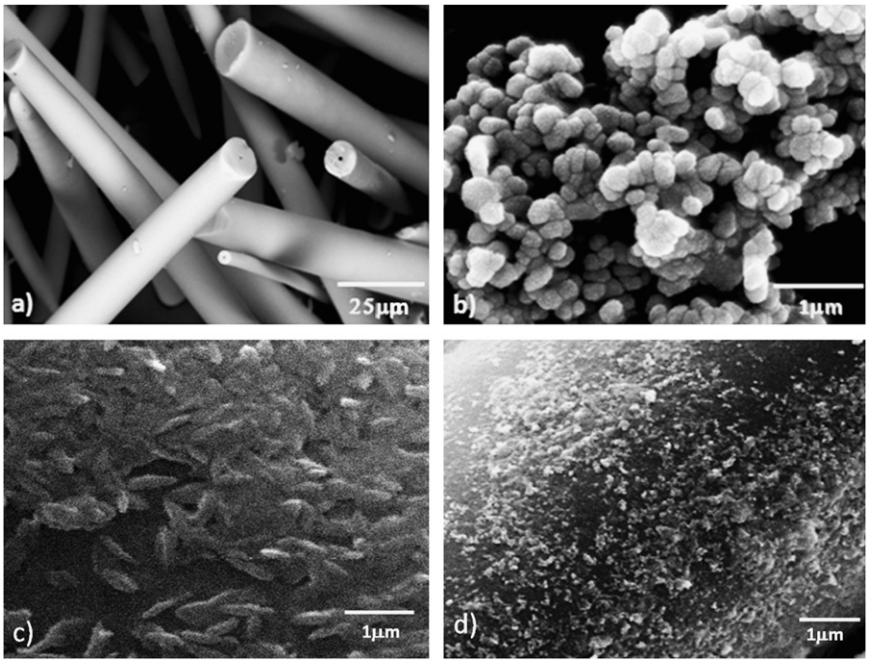

Fig. 3. SEM micrographs of: (a) NAS fibers; (b) commercial nickel oxide; (c) Ni-NAS fibers-wet route and (d) Ni-NAS fibers-dry route. Ni coated NASFs before annealing.

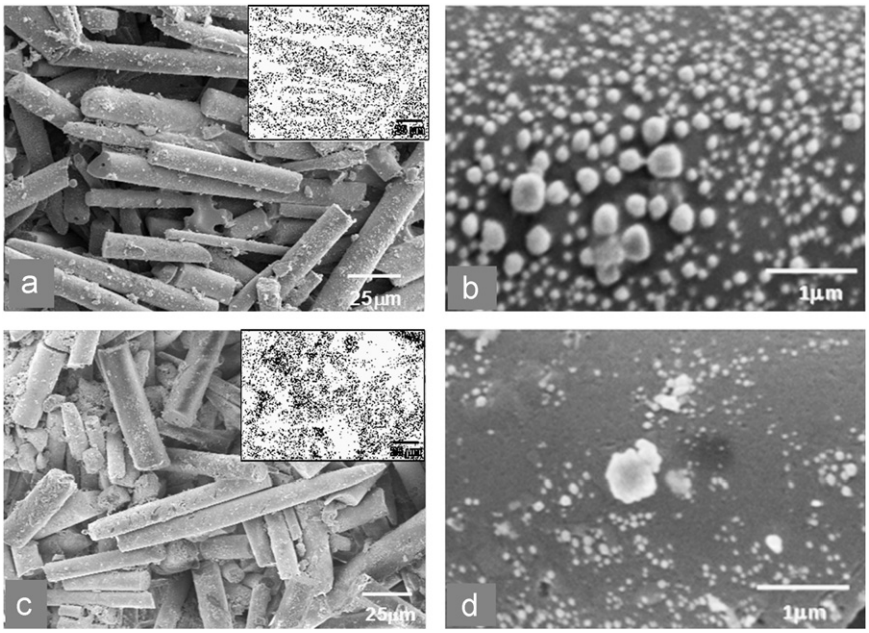

Fig. 4. SEM micrographs of the Ni coated NASFs after annealing. (a) and (b) Ni-NAS fibers-dry route; (c) and (d) Ni-NAS fibers-wet route. Inset in (a) and (c) are EDS color maps of Ni.

Moreover, the Ni particles obtained via wet route are smaller and less dispersed (Fig. 4d). Color mapping of Ni obtained by EDS (inset in Fig. 4a and b) for both samples revealed that Ni obtained from dry route exhibits a higher degree of dispersion, *i.e.* more homogeneously distributed, while Ni obtained by wet route is agglomerated.

A better distribution of the particles on the fibers could be demonstrated by examining the coefficient of variation of the distance between the particles of nickel. The analysis revealed that Ni–SiO_2 fibers prepared by dry routes exhibited a coefficient of variation of the distance between the particles of 0.37, while the value found for Ni–SiO_2 fibers prepared by wet routes was 0.65. The closer to zero is the standard deviation (σ), the more homogeneous is the distribution, *i.e.*, the particles are well dispersed on the fiber surface. Therefore, the higher distribution of particles occurs for Ni–SiO_2 fibers prepared by dry routes.

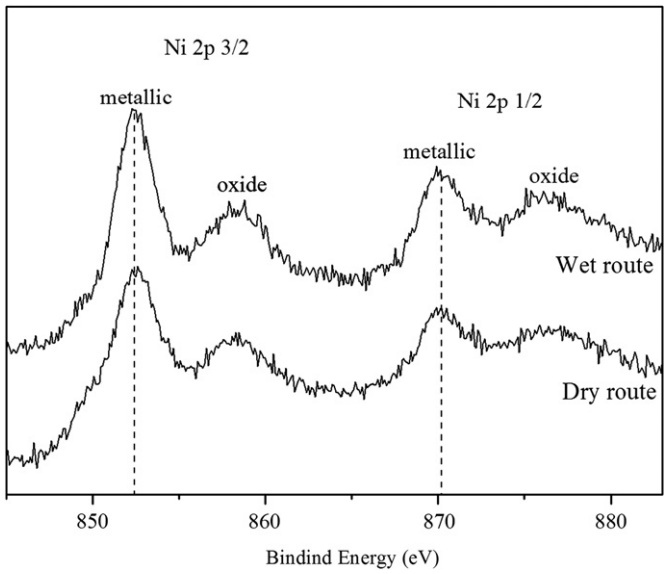

Fig. 5. XPS spectra of Ni 2p from the catalytic filters obtained from: (a) wet and (b) dry routes.

Fig. 5 shows the XPS spectra of Ni 2p from the catalytic filters obtained from both wet and dry routes. Although the precursors were submitted to similar conditions, the XPS results revealed no substantial difference between metallic Ni resulted from both dry and wet routes. The main Ni peaks were identified in both Ni 2p spectra, which are assigned to: metallic nickel (Ni 2p3/2 at 852 eV and Ni 2p1/2 at 870 eV) and its oxidized state (Ni 2p3/2 at 858 eV and Ni 2p1/2 at 876 eV) [29,30]. The amount of metallic nickel on the surface of NASFs represents 44.6% for dry route and 45.1% for wet route, respectively. Moreover, the amount of Ni^0 was higher than oxidized Ni.

Particle size distribution obtained by image analysis—IMAGO® of Ni over the NAS fibers for both wet and dry routes is shown in Fig. 6. Ni particles generated by the dry route are distributed in a broad range of sizes, with mean size of approximately 0.15 μm, while for the Ni–SiO_2 fibers processed by the wet route the majority of Ni particles is significantly smaller with mean size of approximately 0.10 μm, which is in good agreement with the SEM observations (Fig. 4). Additionally, the wet route produced particles with a narrower size distribution.

Table 1 summarizes the physical and mechanical properties (BET total surface area, porosity, pore diameter, tortuosity, Ni-content, Ni-coefficient of variation and compressive strength) of samples obtained by dry and wet routes, as well as of pure SiO_2 fibers filter, as reference. The Ni–SiO_2 fibers produced by wet and dry routes exhibit similar Ni content. The porosity of the Ni–SiO_2 fibers produced by the wet route is slightly lower, probably caused by the clogging of sub-microsized pores by the smaller Ni particles. The compressive strength for all samples is similar (NAS fibers, dry and wet routes). The values of BET surface reveal that the addition of Ni catalyst in the NAS fibers support results in a significant increase on the surface area. Notably, the BET surface area of the Ni–SiO_2 fibers obtained through the wet route is higher than the surface area of the samples produced by the dry route, due to the smaller size of the Ni particles

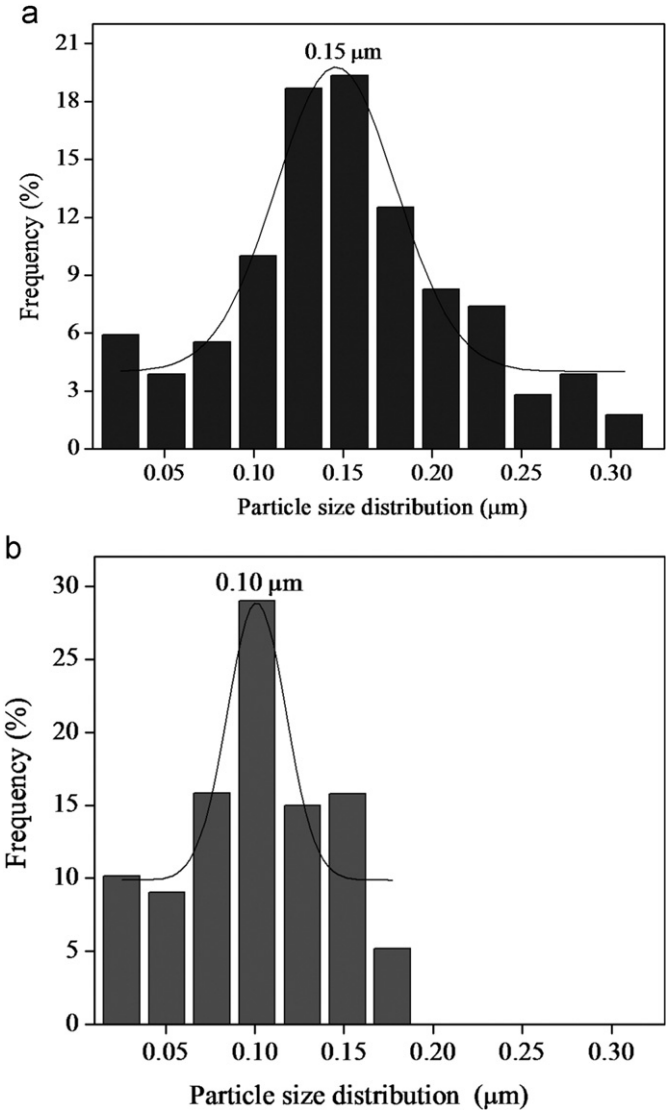

Fig. 6. Ni-particles size distribution: (a) Ni-SiO_2 fibers—dry route and (b) Ni-SiO_2 fibers—wet route.

Table 1
Physical and mechanical properties of catalytic fibrous filters.

Property	Material/support		
	Dry route	Wet route	NASF filter
Ni content (wt%)	3.67	3.98	0
S_{BET} (m^2/g)	4.13	12.2	<0.01
Porosity (%)	64.6 ± 1.3	61.3 ± 1.4	63.9 ± 0.4
Mean pore diameter (μm)	21.86	22.21	20.09
Tortuosity (−)	2.21 ± 0.18	2.34 ± 0.06	1.73 ± 0.01
Ni-coefficient of variation	0.37	0.65	–
Compressive strength (MPa)	1.9 ± 0.3	2.4 ± 0.4	2.4 ± 0.1

resulted from this processing route. The pore diameter of the samples obtained by dry and wet routes is similar to the NAS fibers. The catalytic fibrous filters obtained by dry and wet routes exhibit a larger tortuosity than the SiO_2 fibers. This behavior is probably related to the nickel particles that hinder the gas flow. The Ni–SiO_2 fibers obtained by dry routes revealed a more homogeneous particle distribution than the Ni–SiO_2 fibers obtained by wet route. This behavior might be seen in light of the coefficient of variation of the distance between particles of Ni, as discussed above.

Fig. 7 shows typical pressure drop curves as a function of air velocity at different temperatures. Pressure drop increased with the increase in air velocity, following clear parabolic trends in all cases, which confirmed that Forchheimer's equation fitted better to experimental data than the pure linear relationship stated by Darcy's law.

The increase in air temperature also shifted the pressure drop to higher values and this behavior is related to changes in both fluid and medium properties. Density and viscosity of the gas phase are oppositely affected by temperature, as can be seen in Eqs. (10) and (5). The fact that pressure drop increased with temperature implies in a larger influence of air viscosity changes (represented by the linear term of Eq. (8)) than in air density (represented by the inertial or quadratic term).

Fig. 8 shows the influence of air temperature on the permeability constants, k_1 and k_2, for the catalytic fibrous filters obtained by dry and wet routes. Permeability tests at elevated temperatures revealed the complexity of interactions between the fibrous structure and the gas flow regime. It can be seen in Fig. 8a that the Darcian permeability constant (k_1) tends to be constant with temperature after an initial decrease up to 100 °C. The non-Darcian constant (k_2) (Fig. 8b) exhibits a slight tendency to decrease, up to 430 °C.

Fig. 9 shows the global filtration efficiency of the catalytic fibrous filters obtained by dry and wet routes. According to the Brazilian resolution (CONAMA 403/2008) [31] the maximum emission of pollutants for diesel

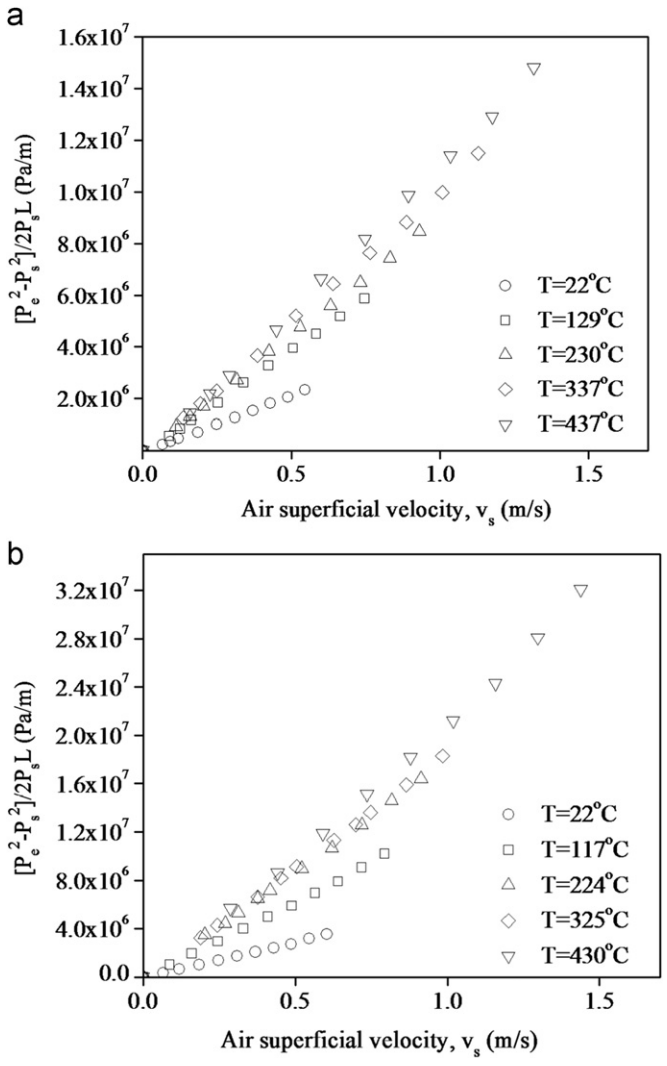

Fig. 7. Pressure drop curves at different temperatures: (a) dry route and (b) wet route.

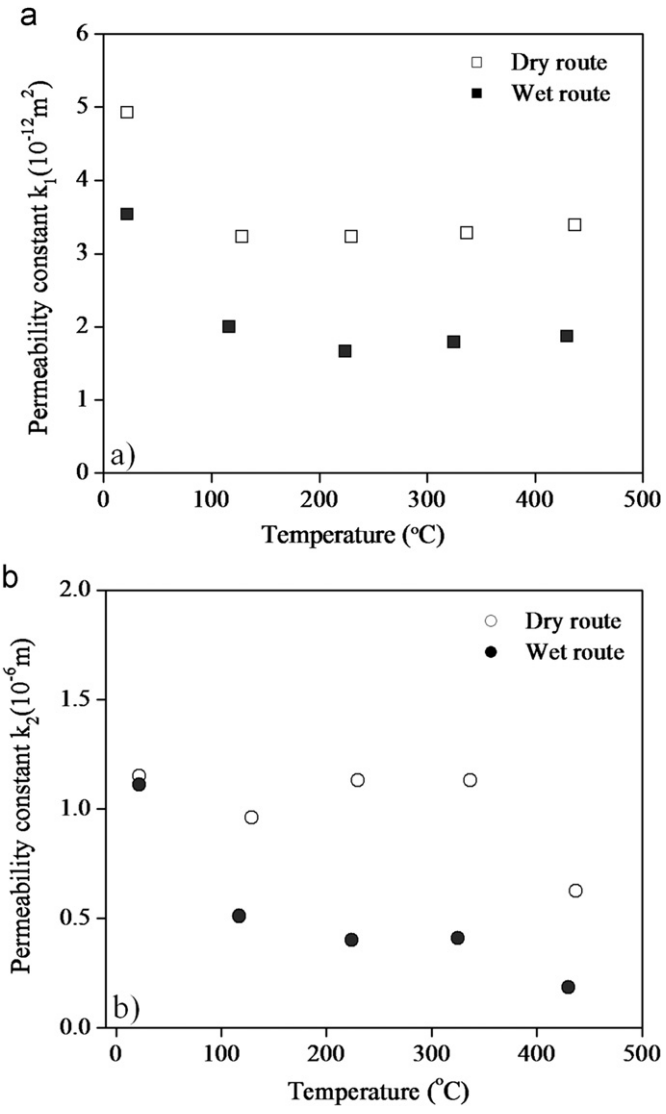

Fig. 8. Influence of testing temperature on the permeability constants: (a) Darcian permeability (k_1) and (b) non-Darcian permeability constant (k_2).

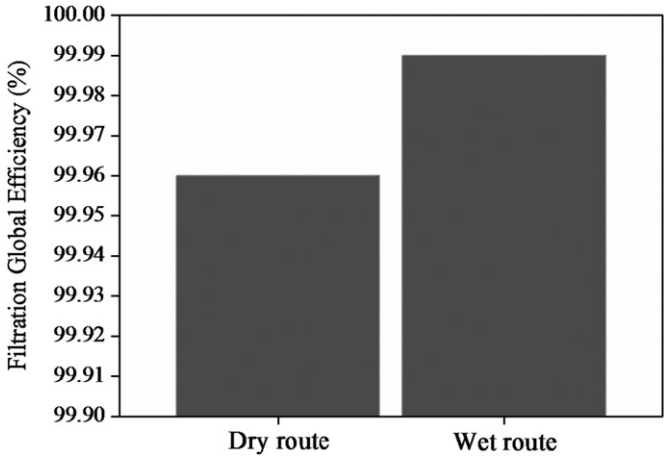

Fig. 9. Global filtration efficiency of catalytic fibrous filters produced by dry and wet routes.

cycle engines of automotive heavy vehicles is limited to a generation rate of particulates in the range 0.02–0.03 g/kw h and according to resolutions CONAMA 415/2009 [32] the maximum emission to light vehicles is limited to a generation rate of particulates in the range 0.025–0.03 g/km [33]. The global efficiency of 99.9%, probably, would be enough to meet the maximum particle emission in diesel engines.

Fig. 10 shows the propylene (C_3H_6), propane (C_3H_8) and carbon monoxide (CO) mass conversion profile as a function of temperature for the catalytic fibrous filters obtained by dry and wet routes. The C_3H_6 mass conversion reactions starts at 150 °C with a low conversion, 14% (dry), and 5% (wet) and increases slowly up to 23% (dry) and 12% (wet) at 300 °C, reaching a conversion of 81% and 53% at 500 °C (Fig. 10a). For propane (Fig. 10b) a similar behavior in the mass conversion reactions occurred, starting with 17 wt% (dry) and 12% (wet) at 150 °C, increasing to 36% (dry) and 14% (wet) at 300 °C and 53% (dry) and 47% (wet) at 500 °C. The conversion of propane is lower than that of propylene for both routes. The possible reactions for the propylene and propane are listed in the chemical reactions from 7 to 10 [34,35]. The catalytic filter produced through the dry route exhibits higher mass conversion to propylene and propane than the filter obtained by the wet route. Catalysis depends not only on the total surface area of the catalyst dispersed over a substrate but also on its degree of dispersion and homogeneity on the surface, which promotes a contact area between the catalyst (Ni) and the gas over the entire support.

$$C_3H_6 + 9/2O_2 \rightarrow 3CO_2 + 3H_2O$$

$$C_3H_8 + 5O_2 \rightarrow 3CO_2 + 4H_2O$$

$$C_3H_6 + 3O_2 \rightarrow 3CO + 3H_2O$$

$$C_3H_8 + 7/2O_2 \rightarrow 3CO + 4H_2O$$

Fig. 10c shows the mass conversion of CO as a function of the temperature. For the dry route the highest gas conversion (reduction) was achieved at 300 °C (32 wt%) and for the wet route the highest value was achieved at 150 °C (36 wt%). At 500 °C for the wet route a

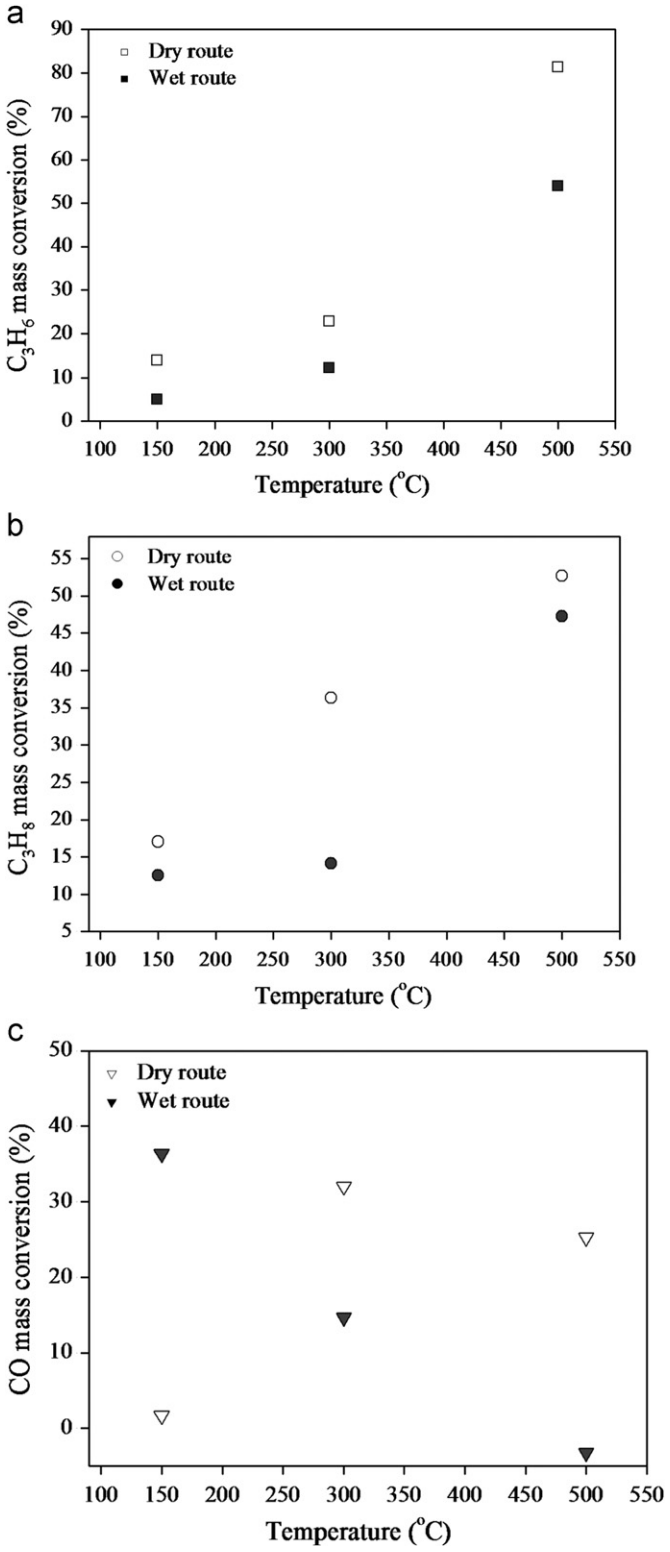

Fig. 10. Mass conversion efficiency of catalytic filters obtained by dry and wet routes for: (a) propylene; (b) propane; and (c) carbon monoxide.

slight increase of the CO occurred. The possible chemical reactions (11) and (12) are represented below [33].

$$CO + 1/2O_2 \rightarrow CO_2$$

$$CO + H_2O \leftrightarrow CO_2 + H_2$$

4. Conclusion

Fibrous Ni-deposited natural amorphous silica catalytic filters were successfully produced through two different techniques named wet and dry routes. Morphological characterization revealed that Ni from wet route was distributed over the silica fibers with significantly lower particle size than the Ni produced through the dry route. Both methods led to a homogeneous distribution of Ni particles over NASF. The catalytic fibrous filter obtained from the dry route showed higher conversion efficiency for both propylene and propane, especially at high temperatures, due to the higher degree of dispersion of Ni particles over the NASF surfaces. Fibrous ceramic with Ni distributed over the fiber surfaces could be used to remove particulates and purify the gases generated in the diesel combustion in a number of applications.

Acknowledgments

The authors thank FAPESC for the financial support under contract PRONEX/FAPESC TO 17431/2011-9. Brazilian Council for Scientific and Technological Development (CNPq) is also acknowledged for scholarships. The authors also gratefully thank Prof. Dr. Wido Herwig Schreiner for XPS measurements and LCME-UFSC for SEM analysis.

References

[1] S. Heidenreich, M. Nacken, M. Hackel, G. Schaub, Catalytic filter elements for combined particle separation and nitrogen oxides removal from gas streams, Powder Technology 180 (2008) 86–90.
[2] U.G. Alkemade, B. Schumann, NO SCR reduction by hydrogen generated in line on perovskite-type catalysts for automotive diesel exhaust gas treatment, Solid State Ionics 177 (2006) 2291–2296.
[3] M.C. Rangel, M.F.A. Carvalho, Impact of automotive catalysts in the control of air quality, Quimica Nova 26 (2003) 265–277.
[4] M.S. Gross, M.A. Ulia, C.A. Querini, Catalytic oxidation of diesel soot: new characterization and kinetic evidence related to the reaction mechanism on K/CeO_2 catalyst, Applied Catalysis A-General 360 (2009) 81–88.
[5] A. Winkler, D. Ferri, M. Aguirre, The influence of chemical and thermal aging on the catalytic activity of a monolithic diesel oxidation catalyst, Applied Catalysis B-Environmental 93 (2009) 177–184.
[6] M. Nacken, S. Heidenreich, M. Hackel, G. Schaub, Catalytic activation of ceramic filter elements for combined particle separation, NO_x removal and VOC total oxidation, Applied Catalysis B-Environmental 70 (2007) 370–376.
[7] Y.A. Kim, J.H. Choi, J. Scott, K. Chiang, R. Amal, Preparation of high porous $Pt–V_2O_5–WO^3/TiO_2/SiC$ filter for simultaneous removal of NO and particulates, Powder Technology 180 (2008) 79–85.
[8] J. Koopa, O. Deutschmann, Detailed surface reaction mechanism for Pt-catalyzed abatement of automotive exhaust gases, Applied Catalysis B-Environmental 91 (2009) 47–58.
[9] N.M. Deraz, M.M. Selim, M. Ramadan, Processing and properties of nanocrystalline Ni and NiO catalysts, Materials Chemistry and Physics 113 (2009) 269–275.
[10] A. Jasik, R. Wojcieszak, S. Monteverdi, M. Ziolek, M.M. Bettahar, Study of nickel catalysts supported on Al_2O_3, SiO_2 or Nb_2O_5 oxides, Journal of Molecular Catalysis A-Chemical 242 (2005) 81–90.
[11] J. Sehested, Frontiers in catalysis: a molecular view of industrial catalysis, Catalysis Today 111 (2006) 103–110.
[12] H.S. Bengaard, J.K. Nørskov, J. Sehested, B.S. Clausen, L.P. Nielsen, A.M. Molenbroek, J.R. Rostrup-Nielsen, Steam reforming and graphite formation on Ni catalysts, Journal of Catalysis 209 (2002) 365–384.
[13] J. Sehested, S. Dahl, J. Jacobsen, J.R. Rostrup-Nielsen, Methods for preparing Ni/Al_2O_3 catalyst, Journal of Physical Chemistry B 109 (2005) 2432–2438.
[14] D.W. Goodman, R.D. Kelley, T.E. Madey, J.T. Yates, Kinetics of the hydrogenation of CO over a single crystal nickel catalyst, Journal of Catalysis 63 (1980) 226–234.
[15] D. Jo, J.S. Lee, K.H. Lee, Enantio-differentiating hydrogenation of methyl acetoacetate over tartaric acid-modified nickel catalysts: effects of preparation method of supported nickel on activity and selectivity of catalysts, Journal of Molecular Catalysis A-Chemical 222 (2004) 199–205.
[16] L. Moldavsky, M. Fichman, C. Gutfinger, Enhancing the performance of fibrous filters by means of acoustic waves, Journal of Aerosol Science 37 (2006) 528–539.
[17] J. Steffens, J.R. Coury, Collection efficiency of fiber filters operating on the removal of nano-sized aerosol particles: I-homogeneous fibers, Separation and Purification Technology 58 (2007) 99–105.
[18] V.A. Kirsch, Stokes flow in model fibrous filters, Separation and Purification Technology 58 (2007) 288–294.
[19] C. Volkmer-Ribeiro, J.F.M. Motta, V.L.M. Callegaro, Taxonomy and Distribution of Brazilian Spongillites. Sponge Sciences-Multidisciplinary Perspectives, in: Y. Watanabe, N. Fusetani (Eds.), Springer Verlang, Tokyo, 1998, pp. 271–278.
[20] C. Volkmer-Ribeiro, J.F.M. Motta, Sponges forming spongilites in ponds and adjacent areas in *Triangulo Mineiro* (*Brazil*), indicating the preservation of habitat, Biociências 3 (1995) 145–169.
[21] M.D.M. Innocentini, P. Sepulveda, F. Ortega, Permeability, in: M. Scheffler, P. Colombo (Eds.), Cellular Ceramics: Structure, Manufacturing, Properties and Applications, Wiley-VCH, USA, 2005, pp. 313–341.
[22] M.D.M. Innocentini, P. Sepulveda, V.R. Salvini, J.R. Coury, V.C. Pandolfelli, Permeability and structure of cellular ceramics: a comparison between two preparation techniques, Journal of the American Ceramic Society 81 (1998) 3349–3352.
[23] D. Hlushkou, U. Tallarek, Transition from creeping via viscous-inertial to turbulent flow in fixed bed, Journal of Chromatography A 1126 (2006) 70–85.
[24] A.E. Scheidegger, The Physics of Flow Through Porous Media, third ed., University of Toronto Press, Canada, 1974.
[25] P. Moldrup, T. Olesen, T. Komatsu, P. Schjønning, D.E. Rolston, Tortuosity, diffusivity and permeability in the soil, liquid and gaseous phases, Soil Science Society of America journal 65 (2001) 613–623.
[26] M.D.M. Innocentini, R.K. Faleiros, R. Pisani Jr., I. Thijs, J. Luyten, S. Mullens, Permeability of porous gelcast scaffolds for bone tissue engineering, Journal of Porous Materials 17 (2010) 615–627.
[27] M. Kaviany, Principles of Heat Transfer in Porous Media, second ed., Springer, New York, 1995.
[28] C.B. I, van, Effect of water vapor on the sintering of glass powder compacts, Journal of the American Ceramic Society 52 (1969) 11–13.
[29] H. Lei, Z. Song, X. Bao, X. Mu, B. Zong, E. Min, XRD and XPS studies on the ultra-uniform Raney-Ni catalyst prepared from the

melt-quenching alloy, Surface and Interface Analysis 32 (2001) 210–213.
[30] I. Czekaj, F. Loviat, F. Raimondi, J. Wambach, S. Biollaz, A. Wokaun, Characterization of surface processes at the Ni-based catalyst during the methanation of biomass-derived synthesis gas: X-ray photoelectron spectroscopy (XPS), Applied Catalysis A-General 329 (2007) 68–78.
[31] CONAMA, National Environmental Council, Resolution no. 403/2008, Brazilian Ministry of the Environment, Brazil, 2008.
[32] CONAMA, National Environmental Council, Resolution no. 415/2009, Brazilian Ministry of the Environment, Brazil, 2009.
[33] D. Fino, G. Saracco, Gas (particulate) filtration, in: M. Scheffler, P. Colombo (Eds.), Cellular Ceramics: Structure, Manufacturing, Properties and Applications, Wiley-VCH, USA, 2005, pp. 416–428.
[34] M.V. Twigg, Progress and future challenges in controlling automotive exhaust gas emissions, Applied Catalysis B-Environmental 70 (2007) 2–15.
[35] J.A. Botas, M.A. Guitiérrez-Ortiz, M.P. González-Marcos, J.A. González-Marcos, J.R. González-Velasco, Kinetic considerations of three-way catalysis in automobile exhaust converters, Applied Catalysis B-Environmental 32 (2001) 243–256.